Comparison of four types of membrane bioreactor systems in terms of shear stress over the membrane surface using computational fluid dynamics

N. Ratkovich and T. R. Bentzen

ABSTRACT

Membrane bioreactors (MBRs) have been used successfully in biological wastewater treatment to solve the perennial problem of effective solids–liquid separation. A common problem with MBR systems is clogging of the modules and fouling of the membrane, resulting in frequent cleaning and replacement, which makes the system less appealing for full-scale applications. It has been widely demonstrated that the filtration performances in MBRs can be greatly improved with a two-phase flow (sludge–air) or higher liquid cross-flow velocities. However, the optimization process of these systems is complex and requires knowledge of the membrane fouling, hydrodynamics and biokinetics. Modern tools such as computational fluid dynamics (CFD) can be used to diagnose and understand the two-phase flow in an MBR. Four cases of different MBR configurations are presented in this work, using CFD as a tool to develop and optimize these systems.

Key words | CFD, rotational MBR, shear stress, side-stream MBR, submerged MBR

N. Ratkovich (corresponding author)
University of Los Andes,
Department of Chemical Engineering,
Product and Process Design Group (GDPP),
Cra 1 No. 18A-12,
Bogota,
Colombia
E-mail: *n.rios262@uniandes.edu.co*

T. R. Bentzen
Aalborg University,
Department of Civil Engineering,
Sohngaardsholmsvej 57,
DK-9000 Aalborg,
Denmark

INTRODUCTION

Bearing in mind the more stringent, effluent quality standards imposed nowadays, treatment efficiencies need to be improved. These improvements can be achieved both in terms of biological removal efficiency as well as in terms of the sludge water separation step. Both can be efficiently achieved in one step by using membrane bioreactors (MBRs), which have proven to be a good alternative to achieve high effluent quality. The design and optimization of MBR units require knowledge of membrane fouling and hydrodynamics. However, most current studies mainly focus on membrane fouling leaving aside the hydrodynamics of the systems despite its crucial role within the MBR system.

Membrane fouling is caused by the attachment of suspended solids and soluble substances on the membrane surface. Different types of fouling can be identified (Judd 2004; Liao *et al*. 2004): (i) clogging is a progressive accumulation of dry sludge in module volume, starting from 'dead zones' in the reactor, (ii) sludging refers to an accumulation of sludge at the surface of the membrane, and (iii) fouling represents all mechanisms of cake building, plus adsorption/blockage into membrane material.

On the other hand, hydrodynamics is of great importance for reducing membrane fouling on the membrane surface (particle deposition as mentioned above). To reduce the fouling on the membrane, there are two options: (i) increase the liquid cross-flow velocity, or (ii) introduce air to create a gas–liquid, two-phase flow. These options are performed to increase the permeate flux, improve membrane rejection characteristics (reduction of fouling) due to a turbulent flow, and increase the surface shear stress and mass transfer for the removal of foulants which are already deposited onto the membrane surface (scouring effect). Membrane performance measured in terms of membrane fouling was observed to be enhanced by gas sparging, and reports have shown improvements up to 63% when air is introduced (Cui & Wright 1996; Berube *et al*. 2006; Bellara 1996). Several mechanisms were identified: (i) bubble-induced secondary flow, (ii) physical displacement of the mass transfer boundary layer, and (iii) pressure pulsing caused by slugs (Cui *et al*. 2003). It has been found that bubbling can limit surface fouling (clogging and sludging), but not internal fouling (adsorption and pore blockage). A comprehensive review of the effects of aeration on submerged MBRs reported that coarse rather than fine bubbling is the preferred mode to control fouling (Cui *et al*. 2003). A general observation is that larger airflow rates decrease the rate at which the pressure rises due to fouling,

doi: 10.2166/wst.2013.515

but that the enhancement reaches a plateau as the gas flow rate increases (Katsoufidou *et al.* 2005). The benefits of bubbling appear to be most effective at low liquid velocities. At high liquid velocities, the performance becomes dominated by bulk liquid shear (Cui *et al.* 2003). Studies on the gas sparging focus on: (1) the effect of overall gas flow rates, (2) bubble size, and (3) frequency (Yeo *et al.* 2006, 2007). When bubbling was applied to the filtration processes, the fluctuation in shear stress affected the flux more than the absolute value of shear stresses induced by the bubbles. The peak of shear stresses induced by bubbling were up to 45% higher compared to when no bubbling was applied (Ducom *et al.* 2002, 2003). It is important to highlight that the effect of shear stresses induced by gas sparging on fouling control is not well understood. As a result, a trial-and-error approach is required in order to find the best air sparging strategies. Nevertheless, the energy used for adding air into the system is a significant component of the operating cost for MBR systems (i.e. up to 40% of the total energy consumption). That is the main reason why hydrodynamic models of MBRs are required to better understand the shear stress induced by high liquid cross-flow velocities and air sparging, and to identify optimal high liquid cross-flow velocities, air sparging scenarios, and membrane module configurations that optimize the magnitude and distribution of shear stress.

Consequently, the effect of the flow regime in the MBR process unit at the macroscale has been an insufficiently known aspect of MBR design. Current methods of design and optimization for a desired flow regime within the MBR systems are largely based on empirical techniques (e.g. specific mixing energy). It is difficult to predict how vessel design in large-scale installations (e.g. size and position of inlets, aeration systems, baffles or membrane orientation) affects the hydrodynamics and, thereby, the overall performance. Therefore, dedicated experiments are needed to fully understand the hydrodynamics of these single- and two-phase flows. Moreover, insight can be obtained using computational fluid dynamics (CFD). CFD hydrodynamic models are commonly used for design and optimization of processes. These hydraulic models of the system in the microscale are required to understand the mechanisms and allow better fouling control. Both microscale and macroscale hydrodynamic investigation can be performed using CFD, which has proven to be a powerful tool for improving design and operation of wastewater treatment systems (Lesjean & Nguyen Cong Duc 2007). This study describes four municipal wastewater treatment MBR cases with CFD models developed for tackling hydrodynamics with different membrane types.

MATERIALS AND METHODS

Case 1 – Side-stream MBR

The AirLift MBR system (X-Flow, Pentair, The Netherlands) consists of membrane modules located outside the bioreactor tank (Figure 1). These membrane modules are arranged vertically and are aerated continuously from the bottom to create an airlift system. The feed pump is only used to overcome hydraulic losses, and the permeation is controlled by a suction pump (Futselaar *et al.* 2007). A module is 3 m high and contains 700 tubes (Figure 1). Each tube has an internal and external diameter of 5.2 and 6 mm, respectively, and the membrane is made of polyvinylidene fluoride (PVDF) with a pore size of 30 nm. The operational parameters of the Airlift system are summarized in Table 1.

The main problem of building a CFD model of the membrane module is drawing and simulating 700 ultrafiltration (UF) membrane tubes. Therefore, only one single UF membrane was modelled to determine the shear stress over the membrane surface, and it is assumed that for each single tube the flow pattern is the same as that described in detail by Ratkovich *et al.* (2009b) and Ratkovich *et al.* (2009a).

Case 2 – Submerged MBR 1

The submerged MBR system (GE – Water and Process Technologies, Oakville, Canada) consists of one cassette with three hollow fiber (HF) ZeeWeed 500c (ZW500) membrane modules. A picture of the cassette with the modules is presented in Figure 2(a). A schematic of the layout of the membrane modules in the pilot system tank and a schematic of the position of the diffusers with respect to the membrane modules are presented in Figures 2(b) and 2(c), respectively. The performance of this pilot system, especially in terms of fouling, has been reported as similar to that of full-scale MBR systems. Therefore, the outcome of this analysis in terms of shear stresses can be considered representative for full-scale systems. Detailed information of the set up can be found in Fulton (2009). The operational parameters of the submerged system are summarized in Table 2.

Case 3 – Submerged MBR 2

The submerged MBR system (AlfaLaval, Denmark) consists of 86 hollow sheet (HS) double-sided polyvinyl membranes, with a total membrane surface of 154 m^2. The air is introduced in the reactor through seven perforated pipes with seven 4 mm

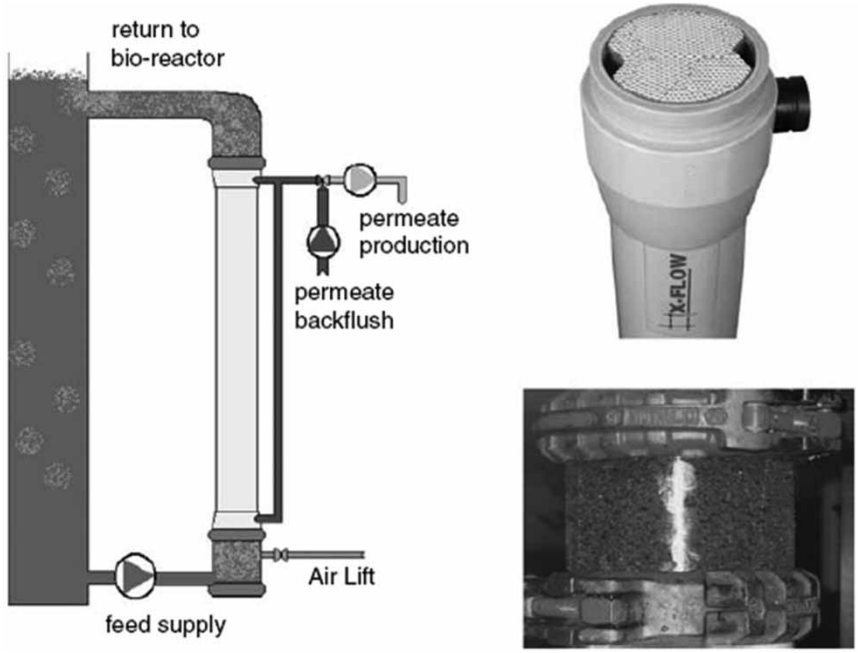

Figure 1 | Basic principle of the Norit AirLift MBR with 8″ X-Flow COMPACT membrane module and continuous aeration (Futselaar *et al*. 2007).

Table 1 | Operational parameters of the Norit Airlift MBR system

Parameter	
Liquid flow rate (m^3/h)	12
Air flow rate (Nm^3/h)	5–10
TSS (g l^{-1})	8–12

holes in each pipe (Figure 3(a)). It operates with a low transmembrane pressure (TMP) (~0.03 bar) across the entire surface of the membrane, and for that reason permeate is drained from the entire surface of the membrane and emerges all the way around the edges, exiting through connectors at the top of the unit (Figure 3(b)). The main advantages of this low TMP are: (1) the membrane is less prone to fouling, resulting in a longer service life between replacement and extended operating periods between cleaning, (2) the activated sludge (AS) passing across the membrane does not accumulate and/or stick to the membrane surface, and (3) the AS flows upwards between the membrane sheets while the permeate passes through the membrane. To ensure that the AS circulates properly, air bubbles are used to create a two-phase cross-flow velocity which, as a side effect, generates a scouring effect that removes the particles attached to the membrane surface. The operational parameters of the submerged system are summarized in Table 3.

Case 4 – Rotational MBR

The rotational cross-flow MBR (Grundfos BioBooster, Denmark) (Figure 4) combines biological treatment with UF membranes, resulting in a stable and high-quality effluent. Rotating cross-flow impellers between the membrane discs prevent fouling and make it possible to operate with a four to five times higher sludge concentration than in conventional MBR systems (TSS up to 40 g l^{-1}). It is important to highlight that those cross-flow impellers ensure low viscosity in the reactor biomass due to the non-Newtonian (NN) behavior of the AS (Rosenberger *et al*. 2002). The operational parameters of the rotational system are summarized in Table 4.

CFD model

The present study describes two types of CFD models: (i) two-phase model for cases 1, 2 and 3, and (ii) a single-phase model for case 4. The objective of these numerical models is to study the hydrodynamics on the systems and more specifically the shear stress over the membrane surface, as the latter is the main indicator on the removal of particles attached to the membrane wall. The implementation was done in Fluent v6.3 (Ansys, USA) for cases 1 and 2, and Star-CCM+ v7.02 (CD-Adapco, UK) for cases 3 and 4. Detailed description of the CFD models can be

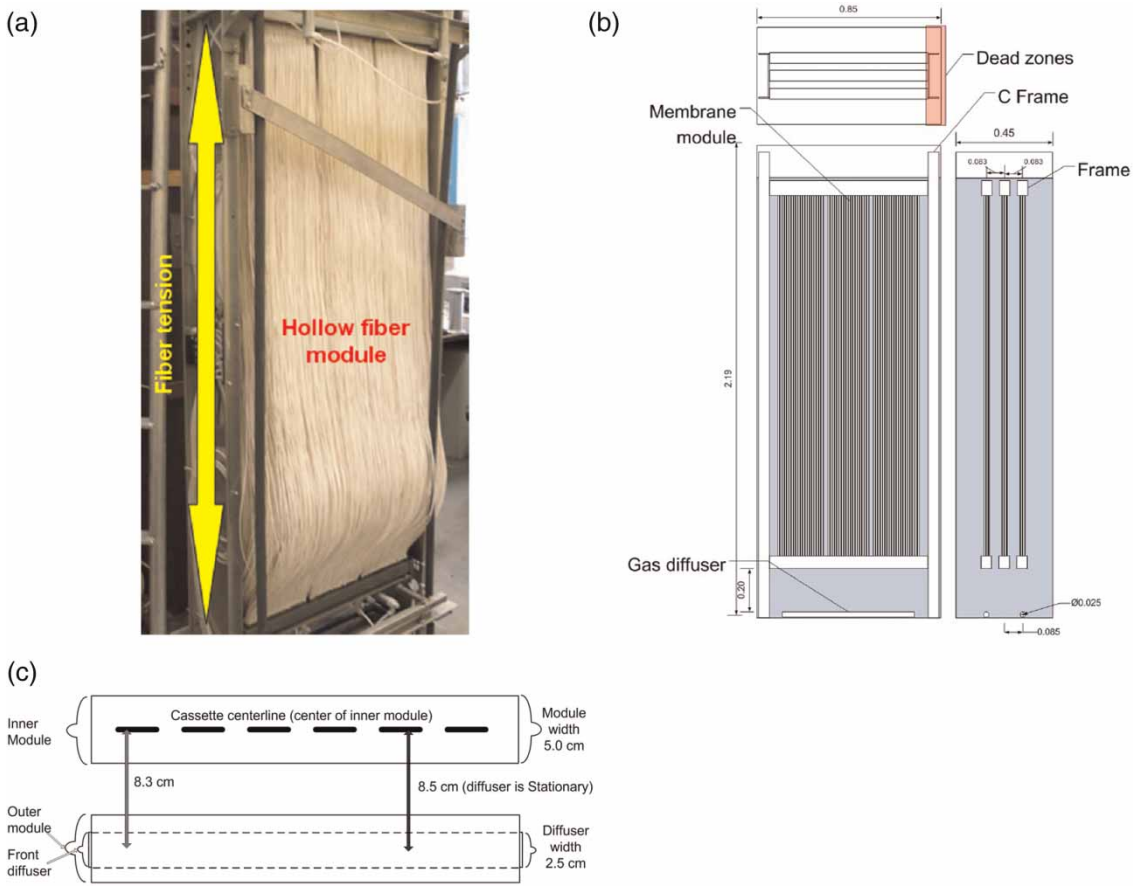

Figure 2 | (a) Cassette frame with membrane modules, (b) membrane module and diffuser location in MBR pilot plant, and (c) location of the diffusers with respect to the membrane modules (Fulton 2009).

Table 2 | Operational parameters of the GE-Zenon MBR system

Parameter	
Air flow rate (Nm^3/h)	5–15
TSS ($g\,l^{-1}$)	8–12

found in Ratkovich *et al.* (2009b) for case 1, Ratkovich *et al.* (2012) for case 2, Bentzen *et al.* (2011) for case 3 and Bentzen *et al.* (2012) for case 4, and it will be not repeated here.

Comparison of experimental measurements with CFD modeling

For cases 1 and 2, experimental shear stress measurements using electrochemical shear probes, were used. From the experiments, a proper validation was attained with CFD. Further details can be found in Ratkovich *et al.* (2009b) and Ratkovich *et al.* (2012), respectively. For case 3, experimental velocity measurements using micro-propellers, were used. From the experiments, a proper validation was attained with CFD in terms of velocity. Therefore, from the CFD models; it was inferred that the shear stress over the membrane surface is accurate (Bentzen *et al.* (2011)). For case 4, experimental velocity measurements using laser doppler anemometry (LDA) were used. From the experiments, a proper validation was attained with CFD in terms of velocity. Therefore, from the CFD models; it was inferred that the shear stress over the membrane surface is accurate (Bentzen *et al.* (2012)).

Viscosity of NN liquids

Viscosity (μ) is a property that influences the hydraulic regime and transport phenomena. It is defined as the ratio between shear stress (τ) and shear rate ($\dot{\gamma}$) as defined by Equation (1).

$$\mu = \frac{\tau}{\dot{\gamma}} \tag{1}$$

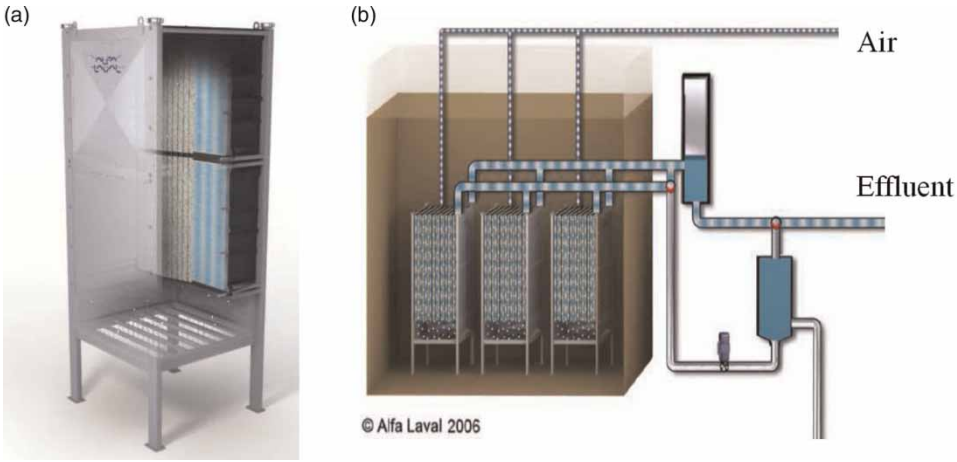

Figure 3 | (a) HS membrane filtration module and (b) submerged MBR.

Table 3 | Operational parameters of the AlfaLaval MBR system

Parameter	
Air flow rate (Nm^3/h)	37–83
TSS ($g\,l^{-1}$)	8–12

The viscosity of Newtonian liquids (e.g. water) exhibits a linear shear stress and shear rate relationship and, thereby, a constant viscosity. However, some particulate suspensions (e.g. AS in MBR) exhibit pseudoplastic (NN) behavior (Rosenberger *et al.* 2002) where the shear stress can be related to the shear rate, according to a power-law relationship as presented in Equation (2).

$$\tau = m\dot{\gamma}^n \tag{2}$$

where m is the flow consistency index ($Pa \cdot s^n$), and n is the flow behavior index (–). For AS in MBR, Rosenberger *et al.* (2002) proposed empirical models for m and n as function of the total suspended solids (TSS in $g\,l^{-1}$), as presented in Equations (3) and (4) respectively.

$$m = 0.001 \exp\left(2\,\mathrm{TSS}^{0.41}\right) \tag{3}$$

$$n = 1 - 0.23\,\mathrm{TSS}^{0.37} \tag{4}$$

Aeration

Aeration is necessary in order to have a scouring effect over the membrane surface (cases 1, 2 and 3). In practice, the membrane aeration value is not defined theoretically since the relationship between aeration and permeate flux decline is currently not well understood (Judd 2001).

For a given aerator system at a fixed depth in the tank, the blower power consumption (E_b in kW) is defined by Equation (5) (Verrecht *et al.* 2008).

$$E_b = \frac{P_{\mathrm{atm}}\, T\, \lambda}{2.73 \cdot 10^5\, \varepsilon\, (\lambda - 1)} \left[\left(\frac{P_{\mathrm{atm}} + \rho_w\, g\, h}{P_{\mathrm{atm}}}\right)^{1-\frac{1}{\lambda}} - 1\right] Q_A \tag{5}$$

where P_{atm} is the atmospheric pressure (=101 325 Pa), T is the inlet temperature (K), ε is the blower efficiency (~0.56),

Figure 4 | (a) Grundfos BioBooster MBR, and (b) close-up of the system.

Table 4 | Operational parameters of the rotational MBR system

Parameter	
Air flow rate (Nm^3/h)	None
Rotational speed (rpm)	150–350
TSS ($g\,l^{-1}$)	8–12

λ is the ratio of specific heat capacity at constant pressure to specific heat capacity at constant volume (c_p/c_v) (=1.4 for air), ρ_w is the density of water (998.28 $kg\,m^{-3}$ at 20 °C), g is the gravity acceleration (=9.81 m^2/s), h is the height of water above the air diffuser (m), and Q_A is the aeration rate (m^3/s).

Liquid cross flow

The liquid flow rate (Q_l) was calculated based on the angular velocity (ω in rpm) of the impeller, the radius r of the impeller (=0.14 m) and the area (A_{gap}) between the impeller, and the membrane (=0.00196 m^2) using Equation (6).

$$Q_l = 120\,\pi\,\omega\,r\,A_{gap} \tag{6}$$

The shaft power consumption (E_s in kW) is defined by Equation (7) for case 4.

$$E_s = \exp(0.0022292205 \cdot \mathrm{TSS}^{1.5} + 0.23705295 \cdot \omega^{1.5} - 4.1925744) \tag{7}$$

Dividing Equations (5) and (7) by the total membrane module area A (m^2) to which the flow rate Q_A or Q_l applies, the power per unit membrane area (W_m in kW/m^2) is then obtained, as presented in Equation (8) (Judd 2001).

$$W_m = \frac{E_i}{A} \tag{8}$$

The sub index i stands for blower (b) or shaft power (S).

RESULTS AND DISCUSSION

The CFD models were simulated with water and not AS. The reason for this is that experimental measurements were only possible with water. Therefore, the CFD models were validated properly with water, and shear stress was obtained. The objective of this study is to convert the shear stress over the membrane surface that was determined for water and to consider the NN behavior of AS in order to compare these four systems.

Based on the air flow rate per unit of membrane area for cases 1, 2 and 3, the different MBR systems were compared. However, air was not introduced into the system in case 4. Therefore, the liquid cross-flow velocity is used for comparison. For the shear stresses of water, the results are presented in Figure 5.

From Figure 5, it is immediately observed that case 4 is less prone to fouling to large wall shear stress values in comparison with cases 1, 2 and 3. To determine the shear stress in the case of AS, the shear rate must be found using Equation (1). Subsequently, it is possible to determine the shear stress using Equations (2), (3) and (4), assuming a TSS of 10 $g\,L^{-1}$. The shear stresses for AS is presented in Figure 6.

As seen in Figures 5 and 6, when comparing the shear stress for water and AS of case 1, there is an increase of 19 times if the NN behavior is considered; for case 2, seven times higher; case 3, four times higher; and case 4, two times higher at low fluid flow rates (<0.52 $m\,h^{-1}$). This shows that the NN behaviors of AS play an important role in hydrodynamics and are related to shear rate, flow behavior and flow consistency index. As observed in Figure 5, the shear stress decreases when the fluid flow rate increases in case 1. That is due to the pulsating nature of the slug flow as the liquid changes direction (up and down) due to the passing of bubbles. It is more likely that higher air flow rates make the water move downwards, decreasing the shear stresses over the membrane surface. However, for the other cases (2, 3 and 4), the shear stress increases when the fluid flow rate increases. In addition, the magnitude of the shear stresses for cases 2 and 3 (both submerged systems), the shear stresses are similar (between 2 to 4 Pa). For case 4, the shear stresses are much larger than in the other systems due to the high liquid rotation. The concavity changes when comparing Figures 5 and 6. Figure 5 presents a concave up-shape, and Figure 6 presents a concave down-shape due to the power-law model of the NN behaviors of AS. The rotation system (case 4) generates higher shear stresses, cf. Figures 5 and 6. It is also important to highlight that the flow rates per unit of membrane area for the systems with aeration (cases 1, 2 and 3) are similar (between 0.15 and 0.60 $m\,h^{-1}$), but for case 4 the range is between 0.6 and 2.8 $m\,h^{-1}$. However, even if large shear stresses are obtained, other aspects need to be considered before issues about fouling can be drawn. Firstly – how sludge characteristics, e.g. floc sizes, bacterial community

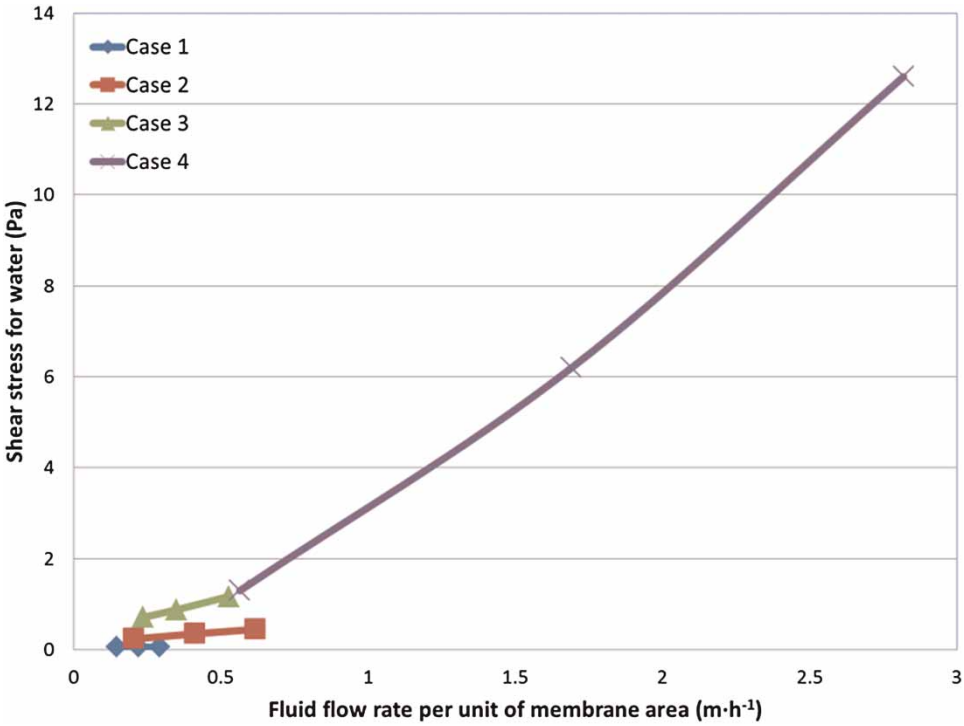

Figure 5 | Fluid flow rate per unit of membrane area vs. shear stress for water.

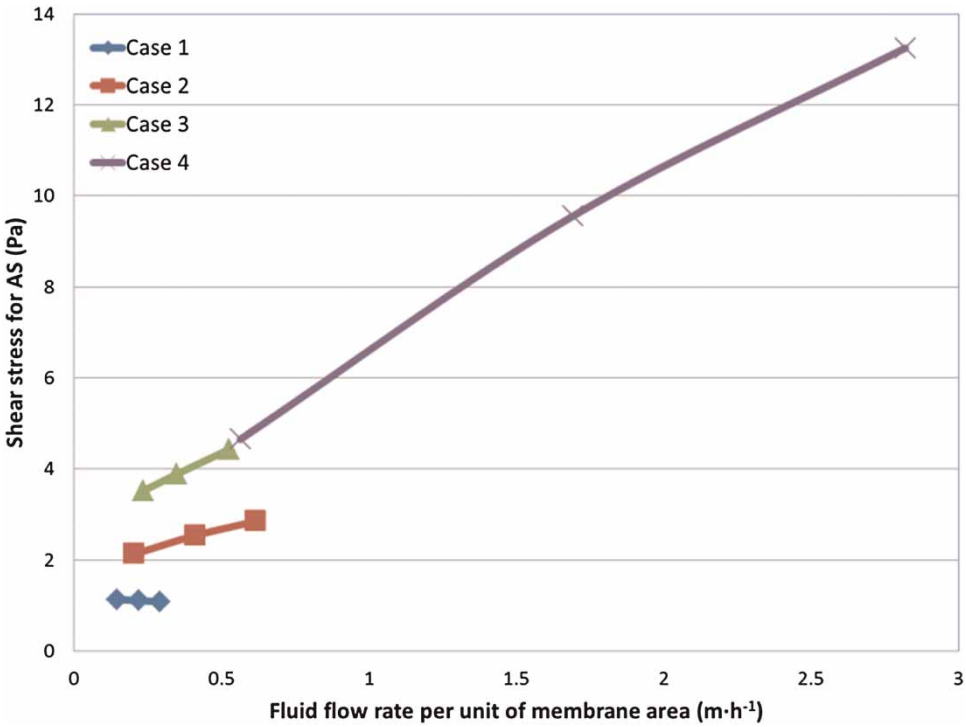

Figure 6 | Fluid flow rate per unit of membrane area vs. shear stress for AS.

is changed due to very high shear rates. Secondly, operational differential pressure will influence the fouling rate, in this respect, case 4 is operating at pressures (up to 4 bars) way above air induces free surface MBR systems.

The system's power consumption depends on viscosity. For the same TSS concentration of 10 g L^{-1} in each case, it is possible to correlate the fluid flow rate with the power consumption using Equation (5) for cases 1, 2 and 3 and Equation (7) for case 4. The results are shown in Figure 7.

From Figure 7, it is observed that cases 1 and 2 have similar power consumption (<0.15 kW). For case 3, the power consumption ranges between 0.35 and 0.85 kW which is roughly four times higher than the other systems with aeration (cases 1 and 2). For case 4, the power consumption reaches up to 1 kW, but the fact that the flow rates are much larger should be considered. However, at low flow rates per unit of membrane area (50 rpm), the power consumption is similar to cases 1 and 2.

Another parameter to consider is the power per unit of membrane area (Equation (8)). The results are shown in Figure 8.

From Figure 8, it is observed that for the systems with aeration (cases 1, 2 and 3) the power consumption per unit on membrane area is in the range between 0.002 and 0.006 kW/m^2. On the other hand, case 4 requires a large amount of power per unit of membrane area to maintain large liquid flow rates. Based on that, case 4 should operate at low rotational speeds (50 rpm) to be similar to the systems with aeration.

Finally, a ratio between the shear stress of AS and power consumption per unit on membrane area should be indicative of which system results prove more efficient. The results are presented in Figure 9.

From Figure 9, it is observed that for all the cases the best ratio of shear per power per membrane area are at low air flow rates (cases 1, 2 and 3) and at low rotational speed (case 4). In addition, cases 1 and 3 produce a similar ratio between shear stress and power (7–15 Pa/kW/m^2). For case 2, which is also a system with aeration and compared to cases 1 and 3, it is roughly three times larger. This means that between the systems with aeration, case 2 will have larger shear stress per unit or power per membrane area. Comparing with case 4, it will produce large ratios at low rotational speeds and will be better than the systems with aeration. The best performing system in terms of ratio of shear per power per membrane area is the case 4 at low rotational speed.

Still there are unknown variables that need to be addressed. The particle size distribution is likely to have

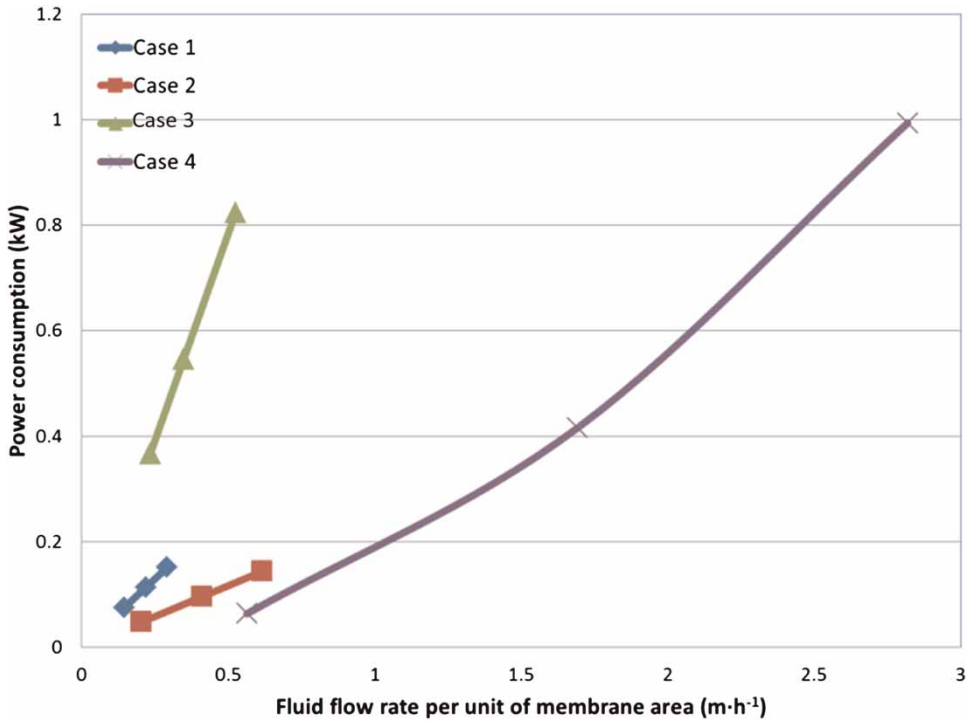

Figure 7 | Fluid flow rate per unit of membrane area vs. power consumption.

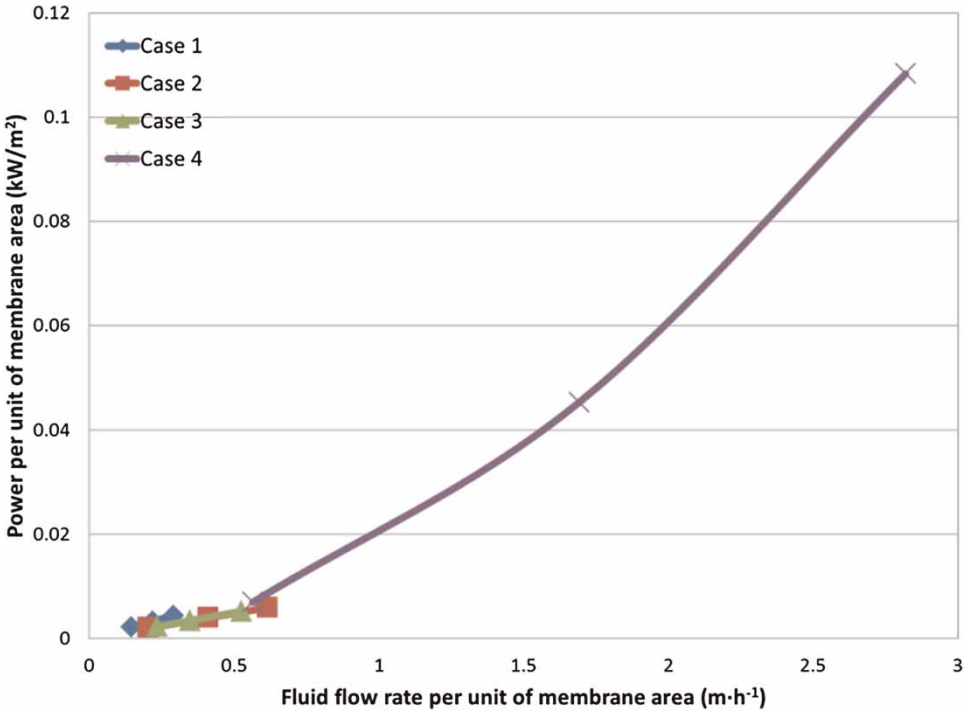

Figure 8 | Fluid flow rate per unit of membrane area vs. power per unit of membrane area.

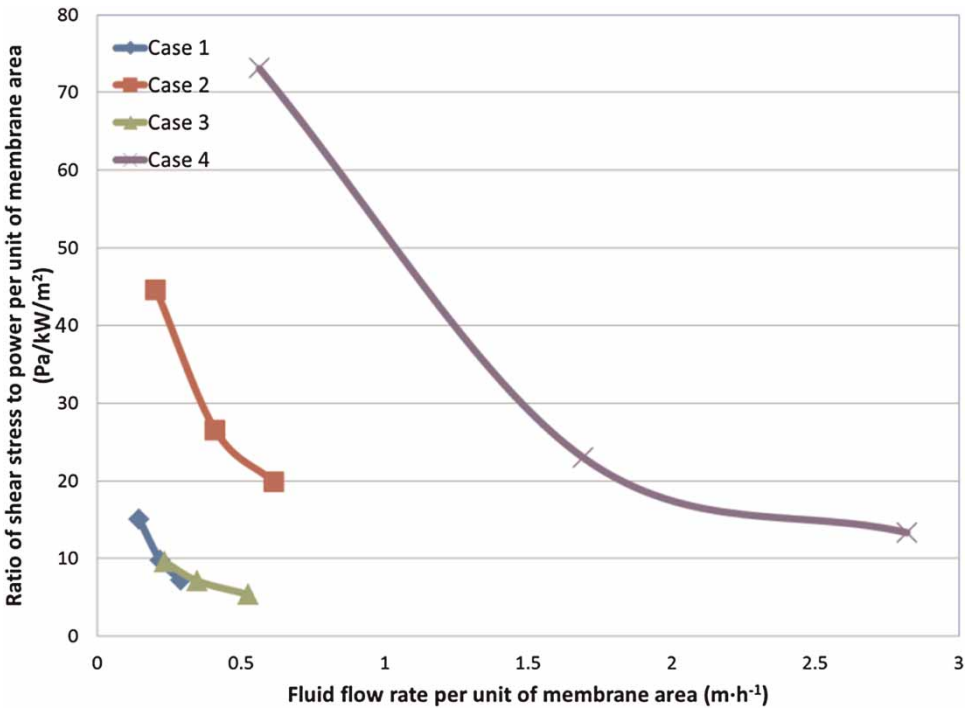

Figure 9 | Fluid flow rate per unit of membrane area vs. ratio between shear stress of AS to power per unit of membrane area.

an impact on sludge viscosity and, hence, the hydrodynamics in MBR systems (Fu & Dempsey 1998; Huisman & Tragasrdh 1999; Jamal Khan *et al.* 2008). Vice versa, hydrodynamics can also impact the particle size distribution through the appearance of shear, which leads to different apparent viscosity of the fluid at different places in the MBR system (Mikkelsen 2001). The main issue is that AS exhibits a non-linear relationship between shear stress and velocity gradients (Rosenberger *et al.* 2002; Hasar *et al.* 2004; Laera *et al.* 2007; Yang *et al.* 2009; Ratkovich *et al.* 2013) which significantly affects the hydrodynamics of MBR systems, the shear stress distribution over the membrane surface and hence, their energy consumption. Indeed, transporting a high viscous fluid over a specific distance will require more energy than transporting plain water along the same distance. Therefore, this will play an important role in designing equipment (such as pumps, mixers, impellers, aeration devices, etc). Hydrodynamics is important for membrane fouling and consequently the permeate flux. The shear stress at the membrane surface affects particles accumulation at the membrane surface (Christensen *et al.* 2009; Bugge *et al.* 2012; Jørgensen *et al.* 2012). Further, the hydrodynamics condition indirectly influences the fouling potential because sludge flocs break-up at high shear stress. This lowers the permeate flux as small particles (colloids) accumulates at the membrane surface (Bacchin *et al.* 2006). However, a thorough description of the relationship between hydrodynamic and fouling is not present in the current state of the art.

CONCLUSIONS

Hydrodynamic CFD models are powerful tools for design and optimization of processes where the value of virtual prototyping has a much lower cost than conducting pilot scale studies and experimentation. Four cases using CFD with different types of membranes were presented in this paper. Case 1 considered a side-stream MBR, and it was found that higher air flow rates decrease shear due to the pulsating nature of slug flow. Cases 2 and 3 considered two submerged MBR systems where the shear stress increases by increasing the air flow rate, and both systems produce similar shear stresses. Finally, case 4, a rotational MBR without injection of air, generates more shear stresses than the other systems.

Performing a comparison of power consumption, it was observed that cases 1 and 2 have similar power consumption. Case 3 has four times more power consumption than cases 1 and 2. In case 4, at low liquid flow rates per unit of membrane area (50 rpm), the power consumption is similar to cases 1 and 2.

In terms of power consumption per unit of membrane area, cases 1, 2 and 3 are similar, but for case 4 it requires a large amount of power per unit of membrane area to maintain large liquid flow rates. Finally, the ratio between shear per power per membrane area was analysed. It was found that cases 1 and 3 produce a similar ratio between shear stress and power. In case 2, it is three times larger than cases 1 and 3, which means that between the systems with aeration, case 2 will have larger shear stress per unit or power per membrane area. Comparing with case 4, it will produce larger ratios at low rotational speeds than the other systems.

REFERENCES

Bacchin, P., Aimar, P. & Field, R. W. 2006 Critical and sustainable fluxes: theory, experiments and applications. *J. Membr. Sci.* **281**, 42–69.

Bellara, S. 1996 Gas sparging to enhance permeate flux in ultrafiltration using hollow fibre membranes. *J. Membr. Sci.* **121**, 175.

Bentzen, T. R., Ratkovich, N., Rasmussen, M. R., Heinen, N. & Hansen, F. 2011 Energy efficient aeration in a single low pressure hollow sheet membrane filtration module. In: G W F – *Wasser, Abwasser*, Vol. 152, No. S1/2011, 2011, pp. 104–107.

Bentzen, T. R., Ratkovich, N., Rasmussen, M. R., Madsen, S., Jensen, J. C. & Bak, S. N. 2012 Analytical and numerical modelling of Newtonian and non-Newtonian liquid in a rotational cross-flow MBR. *Water Sci. Technol.* **66** (11), 2318–2327.

Berube, P. R., Afonso, G., Taghipour, F. & Chan, C. C. V. 2006 Quantifying the shear at the surface of submerged hollow fiber membranes. *J. Membr. Sci.* **279**, 495.

Bugge, T. V., Jørgensen, M. K., Christensen, M. L. & Keiding, K. 2012 Modeling cake buildup under TMP-step filtration in a membrane bioreactor: cake compressibility is significant. *Water Res.* **46**, 4330–4338.

Christensen, M. L., Nielsen, T. B., Andersen, M. B. O. & Keiding, K. 2009 Effect of water-swollen organic materials on crossflow filtration performance. *J. Membr. Sci.* **333**, 94–99.

Cui, Z. F. & Wright, K. I. T. 1996 Flux enhancements with gas sparging in downwards crossflow ultrafiltration: performance and mechanism. *J. Membr. Sci.* **117**, 109.

Cui, Z. F., Chang, S. & Fane, A. G. 2003 The use of gas bubbling to enhance membrane processes. *J. Membr. Sci.* **221**, 1.

Ducom, G., Puech, F. P. & Cabassud, C. 2002 Air sparging with flat sheet nanofiltration: a link between wall shear stresses and flux enhancement. *Desalination* **145**, 97.

Ducom, G., Puech, F. P. & Cabassud, C. 2003 Gas/liquid two-phase flow in a flat sheet filtration module: Measurement of local wall shear stresses. *Can. J. Chem. Eng.* **81**, 771.

Fu, L. F. & Dempsey, B. A. 1998 Modeling the effect of particle size and charge on the structure of the filter cake in ultrafiltration. *J. Membr. Sci*. **149** (2), 221–240.

Fulton, B. 2009 Making membranes more efficient: mapping surface shear in a pilot-scale submerged hollow-fibre membrane cassette using electrochemical shear probes. MASc Thesis, Department of Civil Engineering, The University of British Columbia.

Futselaar, H., Schonewille, H., de Vente, D. & Broens, L. 2007 NORIT AirLift MBR: side-stream system for municipal waste water treatment. *Desalination* **204** (1–3), 1–7.

Hasar, H., Kinaci, C., Ünlü, A., Toğrul, H. & Ipek, U. 2004 Rheological properties of activated sludge in a sMBR. *Biochem. Eng. J*. **20** (1), 1–6.

Huisman, I. & Tragasrdh, G. 1999 Particle transport in crossflow microfiltration – I. Effects of hydrodynamics and diffusion. *Chem. Eng. Sci*. **54** (2), 271–280.

Jamal Khan, S., Visvanathan, C., Jegatheesan, V. & BenAim, R. 2008 Influence of mechanical mixing rates on sludge characteristics and membrane fouling in MBRs. *Sep. Sci. Technol*. **43** (7), 1826–1838.

Judd, S. 2001 Theoretical and experimental representation of a submerged membrane bio-reactor system. *Membr. Technol*. **2001** (135), 4–9.

Judd, S. J. 2004 A review of fouling of membrane bioreactors in sewage treatment. *Water Sci. Technol*. **49**, 229.

Jørgensen, M. K., Bugge, T. V., Keiding, K. & Christensen, M. L. 2012 Modeling approach to determine cake buildup and compression in a high-shear membrane bioreactor. *J. Membr. Sci*. **409–410**, 335–345.

Katsoufidou, K., Yiantsios, S. G. & Karabelas, A. J. 2005 A study of ultrafiltration membrane fouling by humic acids and flux recovery by backwashing: experiments and modeling. *J. Membr. Sci*. **266**, 40.

Laera, G., Giordano, C., Pollice, A., Saturno, D. & Mininni, G. 2007 Membrane bioreactor sludge rheology at different solid retention times. *Water Res*. **41** (18), 4197–4203.

Lesjean, B. & Nguyen Cong Duc, E. 2007 Editors of book of handouts of workshop. In: CFD Modelling for MBR Applications – from the Fibre to the Plant, 3 June 2007, Berlin, Germany. Available for download in www.mbr-network.eu/mbr-projects/downloads-common-details.php?VID=40.

Liao, B. Q., Bagley, D. M., Kraemer, H. E., Leppard, G. G. & Liss, S. N. 2004 A review of biofouling and its control in membrane separation bioreactors. *Water Environ. Res*. **76**, 425.

Mikkelsen, L. M. 2001 The shear sensitivity of activated sludge: relations to filterability, rheology and surface chemistry. *Colloids Surf Physicochem. Eng. Aspects*. **182** (1–3), 1–14.

Ratkovich, N., Hunze, M., Futselaar, H. & Nopens, I. 2009a Use of CFD to model and optimize the hydrodynamics of an airlift MBR side-stream module. *Proceedings of WEFTEC 2009*, October 10–14, 2009, Orlando, FL, USA.

Ratkovich, N., Chan, C. C. V., Berube, P. R. & Nopens, I. 2009b Experimental study and CFD modelling of a two-phase slug flow for an airlift tubular membrane. *Chem. Eng. Sci*. **64**, 3576.

Ratkovich, N. R., Horn, W., Helmus, F., Rosenberger, S., Naessens, W., Nopens, I. & Bentzen, T. R. 2013 Activated Sludge Rheology: a critical review on data collection and modelling. *Water Res*. **47** (2), 463–482.

Ratkovich, N., Hunze, M. & Nopens, I. 2012 Hydrodynamic study of a hollow fiber membrane system using experimentally and numerically derived surface shear stresses. *Multiph. Sci. Technol*. **24** (1), 47–66. DOI: 10.1615/MultScienTechn.v24.i1.20.

Rosenberger, R., Kubin, K. & Kraume, M. 2002 Rheology of activated sludge in membrane bioreactors. *Eng. Life Sci*. **2** (9), 269–275.

Verrecht, B., Judd, S., Guglielmi, G., Brepols, C. & Mulder, J. W. 2008 An aeration energy model for an immersed membrane bioreactor. *Water Res*. **42**, 4761.

Yang, F., Bick, A., Shandalov, S., Brenner, A. & Oron, G. 2009 Yield stress and rheological characteristics of activated sludge in an airlift membrane bioreactor. *J. Membr. Sci*. **334** (1–2), 83–90.

Yeo, A. P. S., Law, A. W. K. & Fane, A. G. 2006 Factors affecting the performance of a submerged hollow fiber bundle. *J. Membr. Sci*. **280**, 969.

Yeo, A. P. S., Law, A. W. K. & Fane, A. G. 2007 The relationship between performance of submerged hollow fibers and bubble-induced phenomena examined by particle image velocimetry. *J. Membr. Sci*. **304**, 125.

First received 2 March 2013; accepted in revised form 15 August 2013. Available online 22 October 2013